Available online at www.sciencedirect.com
ScienceDirect
Polymer 48 (2007) 3003–3012
polymer
www.elsevier.com/locate/polymer

Cyclic viscoplasticity of solid polymers: The effects of strain rate and amplitude of deformation

A.D. Drozdov [a,*], J.deC. Christiansen [b]

[a] Department of Chemical Engineering, Ben-Gurion University of the Negev, P.O. Box 653, Beer-Sheva 84105, Israel
[b] Department of Production, Aalborg University, Fibigerstraede 16, DK-9220 Aalborg, Denmark

Received 26 May 2006; received in revised form 13 March 2007; accepted 14 March 2007
Available online 19 March 2007

Abstract

Observations are reported on polypropylene random copolymer in uniaxial cyclic tensile tests with various strain rates (ranging from 1.7×10^{-4} to 8.3×10^{-3} s^{-1}). Each cycle of deformation involves tension up to the maximal strain ϵ_{max} (from 0.05 to 0.20) and retraction down to the zero stress. The study focuses on deformation programs with 10–50 cycles in each test. A constitutive model is derived for the viscoplastic behavior of a solid polymer at three-dimensional cyclic deformations with small strains. Material constants in the stress–strain relations are found by fitting the experimental data. Good agreement is demonstrated between the observations and the results of numerical simulation.

Keywords: Polypropylene; Viscoplasticity; Cyclic deformation

1. Introduction

This paper is concerned with the viscoplastic response of semicrystalline polymers at cyclic deformations with small strains. Experimental [1–6] and theoretical [7–20] analysis of the mechanical behavior of polymers and polymer composites under cyclic loading has attracted substantial attention in the past decade. This may be explained by development of (i) new areas of industrial applications where cyclic deformations are of primary importance (biomedical devices [5,9]), and (ii) new experimental techniques for the investigation of mechanical properties of polymers (nanoindentation [21]).

The objective of this work is twofold: (i) to report observations in uniaxial cyclic tests on a random copolymer at various strain rates and maximum strains, and (ii) to derive a constitutive model that correctly describes the experimental data.

A polypropylene random copolymer is chosen for the experimental investigation because (i) polypropylene and its derivatives are widely used in industry, and (ii) necking of random copolymers occurs at higher tensile stresses than that of isotactic polypropylene, which allows cyclic tensile tests to be performed in a larger interval of strains.

The necessity to develop a novel constitutive model in cyclic viscoplasticity of solid polymers is explained by the fact that traditional stress–strain relations fail to describe the mechanical response after the first cycle of deformation, see [9,10,13,14,16], to mention a few.

Two starting points in our derivation of a constitutive model should be mentioned. The first is the concept of pseudo-elasticity [22]. We borrow from this theory a hypothesis that some internal parameters in the stress–strain relations may be treated as piecewise constant functions: their values remain constant along each loading and retraction path, but are altered when the strain rate changes its sign. The other starting point is the assumption [11,12] that the strain-rate tensor for plastic deformation is proportional to the strain-rate tensor for macro-deformation (not to the stress tensor as conventional theories presume).

The exposition is organized as follows. Observations in cyclic tensile tests are reported in Section 2. Constitutive

* Corresponding author. Tel.: +972 8 647 2146; fax: +972 8 647 2916.
E-mail address: aleksey@bgumail.bgu.ac.il (A.D. Drozdov).

0032-3861/$ - see front matter © 2007 Elsevier Ltd. All rights reserved.
doi:10.1016/j.polymer.2007.03.038

equations for the viscoplastic response of a polymer at three-dimensional deformations with small strains are developed in Section 3. Adjustable parameters in the stress–strain relations are found in Section 4 by fitting the experimental data. Some concluding remarks are formulated in Section 5.

2. Experimental procedure

Polypropylene random copolymer RF365MO (density 0.905 g/cm^3, melt flow rate 20 g/10 min, yield strain 0.11) was supplied by Borealis A/S (Denmark). Dumbbell specimens for uniaxial tensile tests (ISO standard 527-2) with width 9.85 mm and thickness 3.74 mm were prepared by injection molding.

Mechanical tests were performed at room temperature by using a universal testing machine Instron-5568 equipped with electro-mechanical sensors for the control of longitudinal strains in the active zone of samples. The tensile force was measured by a standard load cell. The engineering stress σ was determined as the ratio of the axial force to the cross-sectional area of specimens in the stress-free state.

Cyclic tensile tests were carried out following a strain-controlled program. In each test, a specimen was stretched with a constant strain rate $\dot{\epsilon}$ up to a maximum strain ϵ_{max}, unloaded down to the zero stress with the strain rate $-\dot{\epsilon}$, reloaded up to the maximum strain with the strain rate $\dot{\epsilon}$, etc. Each test consisted of $N = 10$ cycles and was repeated on three different specimens. To avoid buckling of samples, unloading was performed down to the tensile force 10–15 N (instead of the zero force).

The experimental program involved two series of tests. In the first series, testing was carried out with the maximum strain $\epsilon_{max} = 0.15$ and strain rates 1.7×10^{-4}, 3.3×10^{-4}, 8.3×10^{-4}, 1.7×10^{-3} and 8.3×10^{-3} s^{-1}. In the other series, tests were performed with the strain rate 1.7×10^{-3} s^{-1} and maximum strains 0.05, 0.075, 0.10, 0.125, 0.15, 0.175 and 0.20. These values cover the entire range of strains before necking (necking was observed at the strain $\epsilon \approx 0.22$).

A strain-controlled deformation program is chosen, since this program is widely used for the evaluation of mechanical properties of solid polymers under cyclic loading, see [4–7], to mention a few. The range of strain rates under consideration is dictated by the fact that at strain rates exceeding 10^{-2} s^{-1}, relatively large fluctuations were observed when the sign of strain rate was altered by the testing machine.

The stress–strain diagrams (the engineering stress σ versus engineering strain ϵ) are depicted in Fig. 1 for the first series and in Fig. 2 for the other series of tests. To avoid overlapping of the experimental data, only observations during the first cycle (Fig. 1) and the first two cycles (Fig. 2) are reported. The following conclusions are drawn:

1. The stress–strain diagrams are strongly nonlinear both at loading and retraction.
2. Along the first loading and retraction paths, the engineering stress increases with strain rate.

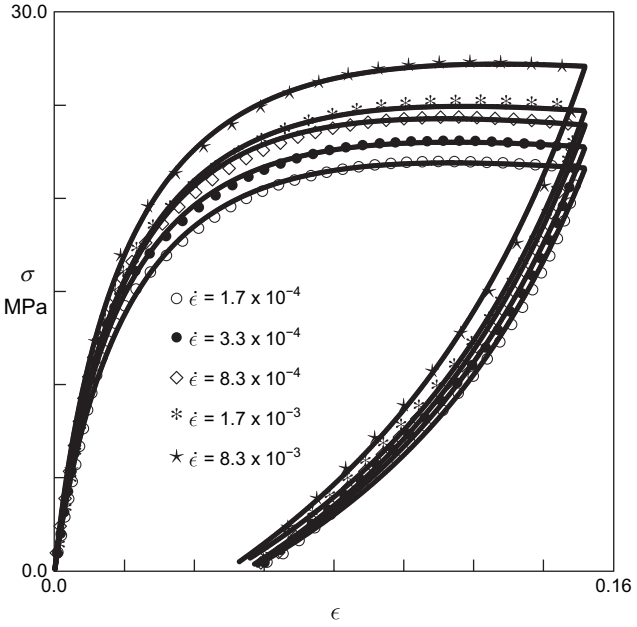

Fig. 1. The engineering stress σ versus engineering strain ϵ in cyclic tensile tests with various strain rates $\dot{\epsilon}$ s^{-1}. Symbols: experimental data. Solid lines: results of numerical simulation.

3. An apparent plastic strain (the strain measured at the instant when the engineering stress vanishes at unloading) is weakly affected by strain rate.
4. The slopes of hysteresis curves strongly decrease, while the hysteresis areas increase with maximum strain.

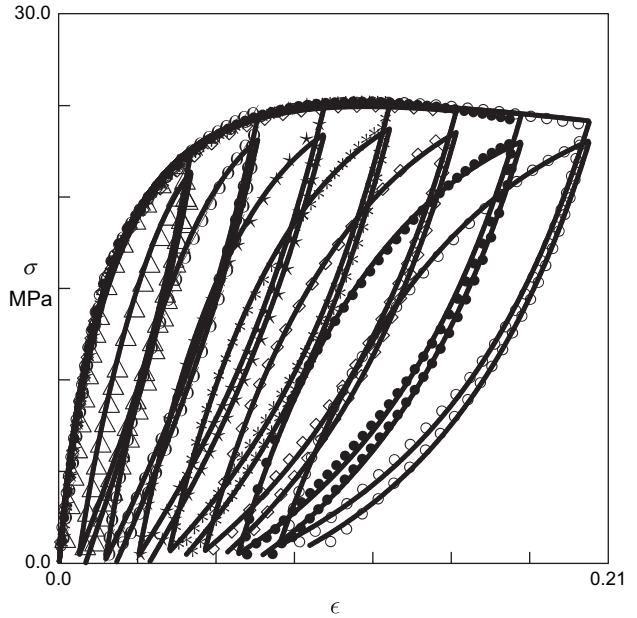

Fig. 2. The engineering stress σ versus engineering strain ϵ in cyclic tensile tests with various maximum strains ($\epsilon_{max} = 0.05$, 0.075, 0.10, 0.125, 0.15, 0.175, 0.20). Symbols: experimental data. Solid lines: results of numerical simulation.

3. A constitutive model

A constitutive model is derived for arbitrary three-dimensional deformations with small strains. The study is confined to cyclic deformations, when the macro-strain tensor $\widehat{\epsilon}(t)$ "increases" from zero at the initial instant $t=0$, reaches its ultimate value $\widehat{\epsilon}_{max}$, "decreases" down to the zero stress tensor, "increases" once more up to $\widehat{\epsilon}_{max}$, and so on.

As the internal structure of a random copolymer is rather complicated, and its detailed description requires a number of experimental parameters, we adopt a phenomenological approach and treat the polymer as an isotropic incompressible medium. Bearing in mind that polypropylene is only slightly compressible (its Poisson's ratio ranges from $\nu=0.43$ [23] to $\nu=0.49$ [24]), the effect of compressibility is disregarded. To simplify the analysis and to reduce the number of material constants, the viscoelastic effects observed in conventional creep and relaxation tests are neglected.

The strain tensor for macro-deformation $\widehat{\epsilon}$ is split into the sum of strain tensors for elastic, $\widehat{\epsilon}_e$, and viscoplastic, $\widehat{\epsilon}_p$, deformations:

$$\widehat{\epsilon}=\widehat{\epsilon}_e+\widehat{\epsilon}_p, \tag{1}$$

where $\widehat{\epsilon}_e$ and $\widehat{\epsilon}_p$ are assumed to be traceless.

We suppose that the rate-of-strain tensor for viscoplastic deformation is proportional to the rate-of-strain tensor for macro-deformation,

$$\frac{d\widehat{\epsilon}_p}{dt}=\phi\frac{d\widehat{\epsilon}}{dt},\quad \widehat{\epsilon}_p(0)=\widehat{0}, \tag{2}$$

where t stands for time, and ϕ is a scalar function to be determined in what follows. The initial condition in Eq. (2) ($\widehat{0}$ stands for the zero tensor) expresses the fact that plastic strain vanishes at the initial instant.

The strain energy (per unit volume) of an isotropic incompressible medium is given by

$$W=\frac{1}{2}\mu\widehat{\epsilon}_e:\widehat{\epsilon}_e, \tag{3}$$

where μ stands for an elastic modulus and colon denotes convolution of tensors. Differentiating Eq. (3) with respect to time and using Eqs. (1) and (2), we find that

$$\frac{dW}{dt}=\mu(1-\phi)\widehat{\epsilon}_e:\frac{d\widehat{\epsilon}}{dt}. \tag{4}$$

At isothermal deformation of an incompressible medium with small strains, the Clausius–Duhem inequality reads

$$Q=-\frac{dW}{dt}+\widehat{\sigma}':\frac{d\widehat{\epsilon}}{dt}\geq 0,$$

where Q stands for energy dissipation per unit time and unit volume, $\widehat{\sigma}$ is the stress tensor, and prime denotes the deviatoric component of a tensor.

Inserting Eq. (4) into this equality and disregarding dissipation of energy, we arrive at the stress–strain relation

$$\widehat{\sigma}(t)=-p(t)\widehat{I}+\mu(1-\phi(t))\big(\widehat{\epsilon}(t)-\widehat{\epsilon}_p(t)\big), \tag{5}$$

where p is an unknown pressure and $\widehat{I}$ stands for the unit tensor.

With reference to the experimental data reported in Section 2, we distinguish between the first loading (when $\widehat{\epsilon}(t)$ changes monotonically from $\widehat{0}$ to some ultimate tensor $\widehat{\epsilon}_{max}$) and subsequent retractions and reloadings. At the first loading, the coefficient ϕ in Eq. (2) is treated as a stretched exponential function of intensity of elastic deformations:

$$\phi=1-\exp\big(-\alpha J_e^{\beta}\big) \tag{6}$$

Here α and β are positive constants, and

$$J_e=\sqrt{\frac{2}{3}\widehat{\epsilon}_e:\widehat{\epsilon}_e}. \tag{7}$$

The choice of Eq. (6) is explained by the fact that it involves only two adjustable parameters. Eq. (6) implies that the rate of viscoplastic strain equals zero at the initial instant, does not exceed the rate of macro-deformation, and reaches the strain rate of macro-deformation at relatively large elastic strains.

Along subsequent paths of retraction and reloading, the pre-factor ϕ obeys the first-order evolution equation

$$\frac{d\phi}{dt}+b|\dot{\epsilon}|\phi=\frac{a}{\mu}\widehat{\sigma}:\frac{d\widehat{\epsilon}}{dt}, \tag{8}$$

where a and b are dimensionless parameters, and $|\dot{\epsilon}|\geq 0$ stands for strain-rate intensity. The initial condition for Eq. (8) is determined by the continuity condition for the function $\phi(t)$. The advantages of Eq. (8) are that it (i) involves only two parameters, a and b, to be determined by matching observations and (ii) contains the work of external forces $\widehat{\sigma}:d\widehat{\epsilon}/dt$ as an input.

With reference to the concept of pseudo-elasticity [22], we suppose that a and b remain constant along each path of a stress–strain diagram at cyclic loading (which means that a and b are constant at each subsequent retraction and reloading), but their values are altered when the strain rate changes its sign. To complete description of the model, it is necessary to define (i) a_+^0, b_+^0 for the first retraction path, i.e., at the first time when $\widehat{\epsilon}=\widehat{\epsilon}_{max}$, (ii) a_-^0, b_-^0 for the first reloading path, i.e., at the first time when the stress tensor $\widehat{\sigma}$ vanishes, and (iii) a rule that allows a_+^0, b_+^0, a_-^0 and b_-^0 to be transformed into the coefficients in Eq. (8) for any subsequent cycle.

Given $\widehat{\epsilon}_{max}$ and $|\dot{\epsilon}|$ (that is when the quantities a_+^0, b_+^0 and a_-^0, b_-^0 are fixed), the dependencies of a and b on these parameters at each subsequent path of retraction and reloading are described by the phenomenological relations

$$a=k_+a_+^0,\quad b=k_+b_+^0\ \text{(retraction)}, \tag{9}$$

$$a=k_-a_-^0,\quad b=k_-b_-^0\ \text{(reloading)}. \tag{10}$$

Eqs. (9) and (10) differ from those introduced in our study on cyclic viscoplasticity of polymer nanocomposites [25].

The coefficients k_+ and k_- are treated as functions of increment of intensity of elastic strain

$$\Delta J_e = J_e - J_e^0, \tag{11}$$

where J_e^0 stands for intensity of elastic strain at the beginning of first retraction (reloading), and J_e is the current intensity of elastic strain when the strain rate changes its sign. The following equations are proposed for k_+ and k_-:

$$k_+ = 1 - K_+\Delta J_e, \quad k_- = k_-^\infty + \left(1 - k_-^\infty\right)\exp\left(-\gamma\Delta J_e\right), \tag{12}$$

where K_+, k_-^∞ and γ are positive quantities.

An advantage of Eqs. (12) is that they contain only three parameters, K_+, k_-^∞ and γ. The first equality implies that $a_+ = a_+^0$ and $b_+ = b_+^0$ for the first retraction path, and a_+ and b_+ decrease linearly with ΔJ_e for subsequent retraction paths. According to the other equality, $a_- = a_-^0$ and $b_- = b_-^0$ for the first reloading path, and a_- and b_- decrease with ΔJ_e exponentially for subsequent reloading paths. When ΔJ_e grows infinitely, the last equality in Eqs. (12) implies that a_- and b_- tend to $k_-^\infty a_-^0$ and $k_-^\infty b_-^0$, respectively.

Eqs. (12) are applicable for low-cycle deformation programs, when ΔJ_e remains small compared with unity. However, the first equality in Eqs. (12) loses its physical meaning at high-cycle programs if the coefficient k_+ becomes negative due to growth of ΔJ_e. To avoid this inconsistency, we postulate that Eqs. (12) are satisfied at $\Delta J_e \le \Delta J_e^{cr}$ only, where ΔJ_e^{cr} is the critical increment of elastic strain. When ΔJ_e exceeds ΔJ_e^{cr} (high-cycle deformation programs), the coefficients k_+ and k_- remain constant.

Given an ultimate strain tensor $\widehat{\epsilon}_{max}$ and a strain-rate intensity $|\dot{\epsilon}|$, constitutive equations (1)–(12) involve nine parameters

$$\mu, \alpha, \beta, a_+^0, b_+^0, a_-^0, b_-^0, K_+, k_-^\infty, \gamma \tag{13}$$

for a low-cycle deformation program and 10 adjustable parameters (the above quantities and ΔJ_e^{cr}) for a high-cycle program.

Our aim now is to describe how these parameters are affected by strain rate and maximum strain per cycle.

3.1. Effect of strain rate

To describe the effect of strain rate on material parameters, we postulate that the μ weakly increases with strain rate intensity,

$$\mu = \mu_0 + \mu_1 \ln|\dot{\epsilon}|, \tag{14}$$

where μ_0 and μ_1 are material constants. Eq. (14) is widely used to account for changes in elastic moduli driven by an increase in strain rate [26,27]. It should be noted that this formula is valid in a limited interval of strain rates only, and it cannot be extrapolated to $\dot{\epsilon} \to 0$.

By analogy with Eq. (14), the following equation is suggested for the influence of strain rate on the dimensionless parameter α:

$$\alpha = \alpha_0 - \alpha_1 \ln|\dot{\epsilon}|, \tag{15}$$

where α_m ($m = 0, 1$) are material constants. The exponent β in Eq. (6) is independent of strain rate

$$\beta = \beta_0. \tag{16}$$

To explain the physical meaning of Eqs. (15) and (16), we concentrate on uniaxial tensile deformation with $J_e = \epsilon_e$ and re-write Eq. (6) in the form

$$\phi = 1 - \exp\left[-\left(\frac{\epsilon_e}{\epsilon_*}\right)^\beta\right], \tag{17}$$

where $\epsilon_* = (1/\alpha)^{1/\beta}$ may be associated with the yield strain. At relatively small strain rates, combination of Eqs. (15)–(17) implies that

$$\epsilon_* = \epsilon_*^{(0)} + \epsilon_*^{(1)} \ln|\dot{\epsilon}|$$

with

$$\epsilon_*^{(0)} = \left(\frac{1}{\alpha_0}\right)^{\frac{1}{\beta_0}}, \quad \epsilon_*^{(1)} = \frac{\alpha_1}{\alpha_0\beta}.$$

Assuming the yield stress σ_* to be proportional to the yield strain ϵ_*, we arrive at the Eyring law

$$\sigma_* = \sigma_*^{(0)} + \sigma_*^{(1)} \ln|\dot{\epsilon}|,$$

whose validity has been confirmed by experimental data, see [28] and the references therein.

Similarly to Eq. (15), we suppose that a_+^0, b_+^0, a_-^0 and b_-^0 decrease linearly with logarithm of strain rate

$$a_+^0 = A_{0+} - A_{1+}\ln|\dot{\epsilon}|, \quad b_+^0 = B_{0+} - B_{1+}\ln|\dot{\epsilon}|,$$
$$a_-^0 = A_{0-} - A_{1-}\ln|\dot{\epsilon}|, \quad b_-^0 = B_{0-} - B_{1-}\ln|\dot{\epsilon}|, \tag{18}$$

where the coefficients A_{m+}, A_{m-}, B_{m+} and B_{m-} ($m = 0, 1$) are independent of $\dot{\epsilon}$.

The quantities K_+, k_-^∞ and γ in Eqs. (12) are independent of strain rate.

Given an ultimate strain tensor $\widehat{\epsilon}_{max}$, the set of material constants for cyclic deformations with various strain rates involves 16 parameters

$$\mu_0, \mu_1, \alpha_0, \alpha_1, \beta_0, A_{0+}, A_{1+}, B_{0+}, B_{1+}, A_{0-}, A_{1-}, B_{0-}, B_{1-}, K_+, k_-^\infty, \gamma. \tag{19}$$

3.2. Effect of maximum strain

As μ, α and β describe the mechanical response at first loading, they are independent of maximum strain per cycle. The other parameters are affected by maximum strain intensity J_e reached at the first loading (retraction). The quantities a_+^0, b_+^0, a_-^0 and b_-^0 decrease exponentially with J_e,

$$\ln a_+^0 = A_{0+} - A_{1+}J_e, \quad \ln b_+^0 = B_{0+} - B_{1+}J_e,$$
$$\ln a_-^0 = A_{0-} - A_{1-}J_e, \quad \ln b_-^0 = B_{0-} - B_{1-}J_e, \tag{20}$$

where A_{m+}, A_{m-}, B_{m+} and B_{m-} ($m = 0, 1$) are constants. Eqs. (20) are similar to the relations suggested in [29] for cyclic deformations of particle-reinforced rubbers within the concept of pseudo-elasticity.

The parameter γ in Eq. (12) is not affected by maximum strain, whereas evolution of K_+ and k_-^∞ with J_e is described by the equations

$$\ln K_+ = K_{0+} - K_{1+}J_e, \quad k_-^\infty = K_-^\infty J_e, \tag{21}$$

where K_{0+}, K_{1+} and K_-^∞ are independent of J_e.

Given a strain-rate intensity $|\dot{\epsilon}|$, the set of material constants for cyclic deformations with various maximum strains involves 15 parameters

$$\mu, \alpha, \beta, A_{0+}, A_{1+}, B_{0+}, B_{1+}, A_{0-}, A_{1-}, B_{0-}, B_{1-}, K_{0+}, K_{1+}, K_-^\infty, \gamma. \tag{22}$$

The number of experimental constants in the model is comparable with that in the stress–strain relations proposed by other researchers (7 in [13,14], 10 in [17], 12 in [15], 12–15 in [9,10], 15 in [16]). An advantage of the constitutive equations is that (i) they can describe the mechanical response in cyclic tests with an arbitrary number of cycles, and (ii) material constants can be found one after another in such a way that no more than three parameters are determined by using observations along each reloading (retraction) path.

4. Determination of material parameters

Determination of experimental constants provides the main source of difficulties in application of conventional models in cyclic viscoplasticity, as a large number of parameters is to be found simultaneously by matching (relatively small) intervals of a stress–strain diagram. Our aim now is to demonstrate how adjustable parameters in the constitutive equations can be determined by fitting the experimental data reported in Section 2.

4.1. Uniaxial cyclic tests

First, we simplify the constitutive equations for uniaxial tension of a specimen, when the strain tensor for macrodeformation reads

$$\widehat{\epsilon} = \epsilon(t)\left[\mathbf{e}_1 \otimes \mathbf{e}_1 - \frac{1}{2}(\mathbf{e}_2 \otimes \mathbf{e}_2 + \mathbf{e}_3 \otimes \mathbf{e}_3)\right]. \tag{23}$$

Here $\epsilon(t)$ stands for longitudinal engineering strain, $\mathbf{e}_k$ ($k = 1, 2, 3$) are unit vectors of a Cartesian frame, whose vector $\mathbf{e}_1$ coincides with the direction of loading, and $\otimes$ denotes tensor product. Assuming the plastic strain tensor $\widehat{\epsilon}_p$ to be presented in the form (23),

$$\widehat{\epsilon}_p = \epsilon_p(t)\left[\mathbf{e}_1 \otimes \mathbf{e}_1 - \frac{1}{2}(\mathbf{e}_2 \otimes \mathbf{e}_2 + \mathbf{e}_3 \otimes \mathbf{e}_3)\right], \tag{24}$$

where $\epsilon_p(t)$ is a function to be found, we substitute Eqs. (23), (24) and (7) into Eqs. (2) and (6) and find that

$$\frac{d\epsilon_p}{d\epsilon} = \phi, \quad \epsilon_p(0) = 0, \tag{25}$$

where

$$\phi = 1 - \exp\left[-\alpha(\epsilon - \epsilon_p)^\beta\right]. \tag{26}$$

Inserting expressions (23), (24) and (7) into Eq. (5) and excluding pressure p from the boundary condition on the lateral surface of a specimen, we calculate the engineering tensile stress σ,

$$\sigma = E\Sigma, \quad \Sigma = (1 - \phi)(\epsilon - \epsilon_p), \tag{27}$$

where $E = 3/2\mu$ stands for an analog of the Young's modulus.

4.2. Tension of a virgin sample

The quantities E, α and β are determined by matching the first loading path of a stress–strain curve with the help of the following algorithm. We fix some intervals $[0, \alpha_0]$ and $[0, \beta_0]$, where the best-fit parameters α and β are located and divide these intervals by the points $\alpha_i = i\Delta\alpha$ and $\beta_j = j\Delta\beta$, where $\Delta\alpha = \alpha_0/J$ and $\Delta\beta = \beta_0/J$ ($i, j = 1,\ldots, J-1$). For each pair $\{\alpha_i, \beta_j\}$, Eqs. (25) and (26) are integrated numerically (by the Runge–Kutta method with the step $\Delta\epsilon = 1.0 \times 10^{-5}$) from $\epsilon = 0$ to ϵ_{max}. The pre-factor E in Eq. (27) is found by the least-squares method from the condition of minimum of the function

$$\mathcal{F} = \sum_n \left(\sigma_{exp}(\epsilon_n) - \sigma_{num}(\epsilon_n)\right)^2,$$

where the sum is calculated over all points ϵ_n at which observations are reported, σ_{exp} is the stress measured in the test, and σ_{num} is given by Eq. (27). The best-fit values $\overline{\alpha}$ and $\overline{\beta}$ are chosen from the condition of minimum of $\mathcal{F}$ on the set of pairs $\{\alpha_i, \beta_j\}$.

After finding $\overline{\alpha}$ and $\overline{\beta}$, the initial intervals $[0, \alpha_0]$ and $[0, \beta_0]$ are replaced with the new intervals $[\overline{\alpha} - \Delta\alpha, \overline{\alpha} + \Delta\alpha]$ and $[\overline{\beta} - \Delta\beta, \overline{\beta} + \Delta\beta]$, and the calculations are repeated. To ensure an acceptable quality of fitting observations, this procedure is repeated three times with $J = 10$.

We begin with matching the experimental data obtained in the first series of tests (cyclic deformations with the maximal strain $\epsilon_{max} = 0.15$ and various strain rates). The loading path of each stress–strain diagram is approximated separately (Fig. 3). For the sake of brevity, we report the experimental data obtained in a cyclic test with a strain rate of 1.7×10^{-3} s^{-1} only. The quality of fitting observations at cyclic deformations with other strain rates is similar. The best-fit parameters E, α and β are plotted versus strain rate $|\dot{\epsilon}|$ in Figs. 4 and 5 together with their approximations by Eqs. (14)–(16). The quantities E_0, E_1, α_0, α_1 and β_0 are collected in Table 1.

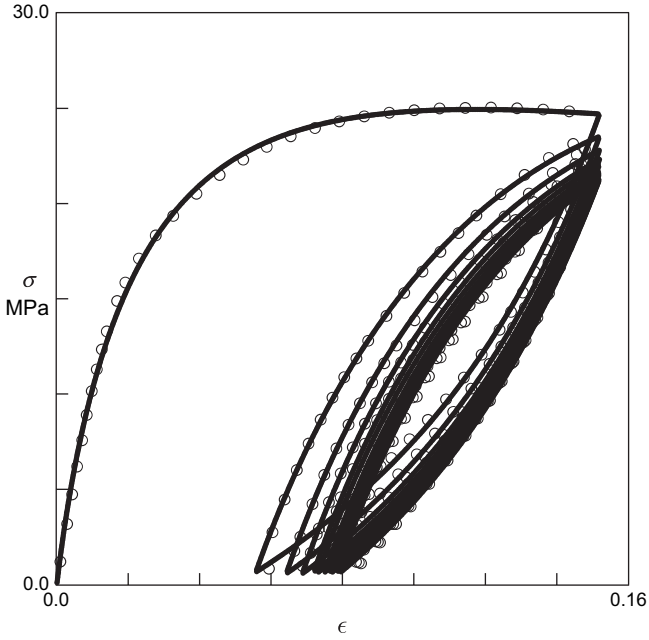

Fig. 3. The engineering stress σ versus engineering strain ϵ in a cyclic tensile test with a strain rate of 1.7×10^{-3} s^{-1}. Circles: experimental data. Solid line: results of numerical simulation.

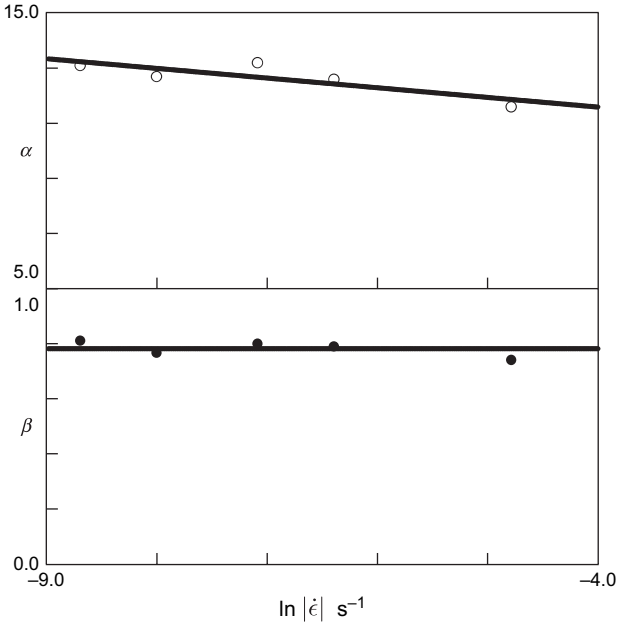

Fig. 5. Adjustable parameters α and β versus strain rate $\dot{\epsilon}$. Symbols: treatment of observations in cyclic tensile tests with various strain rates. Solid lines: approximation of the experimental data by Eqs. (15) and (16).

4.3. First retraction

To find other parameters of the model, we approximate the first retraction path of each stress–strain curve. Using Eqs. (23) and (27), we present Eq. (8) in the form

$$\frac{d\phi}{d\epsilon} = a\Sigma + b\phi. \tag{28}$$

To find a_+^0 and b_+^0, we fix some intervals $[0, a_0]$ and $[0, b_0]$, where these quantities are located, and divide these intervals by the points $a_i = i\Delta a$ and $b_j = j\Delta b$ with $\Delta a = a_0/J$, $\Delta b = b_0/J$ ($i, j = 1,\ldots, J-1$). For any pair $\{a_i, b_j\}$, Eqs. (25), (27) and (28) are integrated numerically (by the Runge–Kutta method with the step $|\Delta\epsilon| = 1.0 \times 10^{-5}$) from $\epsilon = \epsilon_{max}$ to $\sigma = 0$. The initial conditions for Eqs. (25) and (28) reflect

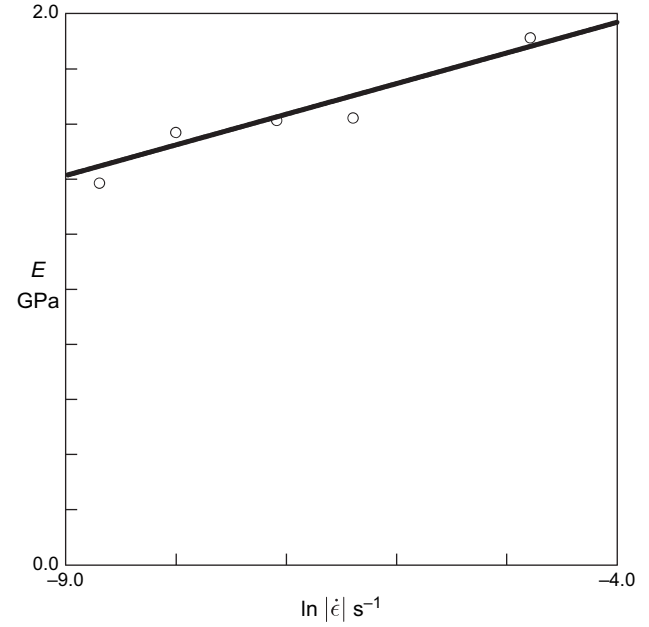

Fig. 4. The elastic modulus E versus strain rate $\dot{\epsilon}$. Circles: treatment of observations in cyclic tensile tests with various strain rates. Solid line: approximation of the experimental data by Eq. (14).

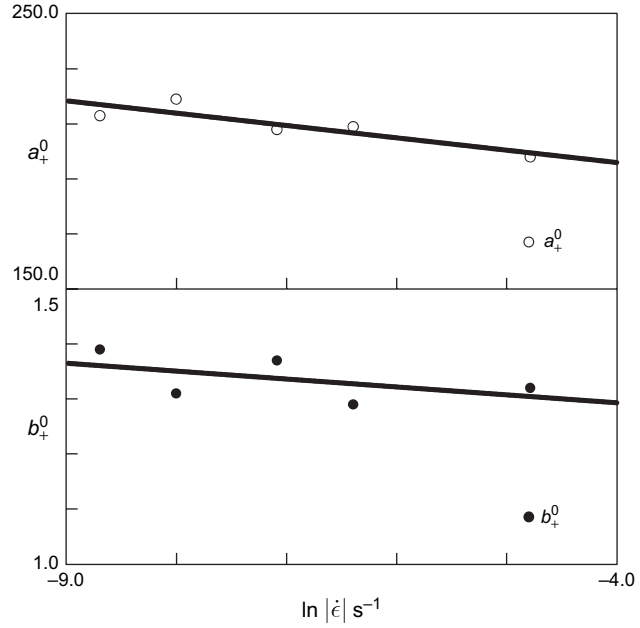

Fig. 6. Adjustable parameters a_+^0 and b_+^0 versus strain rate $\dot{\epsilon}$. Symbols: treatment of observations in cyclic tensile tests with various strain rates. Solid lines: approximation of the experimental data by Eq. (18).

Table 1
Adjustable parameters of the model for cyclic tests with a constant maximum strain $\epsilon_{max} = 0.15$ and various strain rates

Parameter	Value
E_0 (GPa)	2.41
E_1 (GPa)	0.11
α_0	10.19
α_1	0.35
β	0.78
A_{0+}	178.03
A_{1+}	4.48
B_{0+}	1.24
B_{1+}	0.01
A_{0-}	238.53
A_{1-}	19.05
B_{0-}	3.84
B_{1-}	0.39
γ	40.70
K_+	7.45
k_-^∞	0.48

continuity of the functions $\epsilon_p(\epsilon)$ and $\phi(\epsilon)$. The best-fit parameters $\overline{a}_+$ and $\overline{b}_+$ are determined from the condition of minimum of $\mathcal{F}$ on the set $\{a_i, b_j\}$. Afterwards, the initial intervals [0, a_0] and [0, b_0] are replaced with $[\overline{a}_+ - \Delta a, \overline{a}_+ + \Delta a]$ and $[\overline{b}_+ - \Delta b, \overline{b}_+ + \Delta b]$, and the calculations are repeated. This procedure is repeated three times with $J = 10$.

When the best-fit values of a_+^0 and b_+^0 are found, these quantities are plotted versus strain rate $|\dot{\epsilon}|$ in Fig. 6 together with their approximations by Eqs. (18), where the coefficients A_{0+}, A_{1+}, B_{0+} and B_{1+} are determined by the least-squares technique. These coefficients are collected in Table 1.

4.4. Second cycle of deformation

Adjustable parameters a_-^0, b_-^0 and k_+ are found by fitting observations at the second cycle of deformation using the following algorithm. First, we re-write Eq. (8) for reloading in the form

$$\frac{d\phi}{d\epsilon} = a\Sigma - b\phi. \tag{29}$$

We fix some intervals [0, a_0] and [0, b_0], where the best-fit parameters a_-^0 and b_-^0 are assumed to be located, and the interval [0, 1] for the parameter k_+. These intervals are divided by the points $a_i = i\Delta a$, $b_j = j\Delta b$ and $k_l = l\Delta k$ with $\Delta a = a_0/J$, $\Delta b = b_0/J$ and $\Delta k = 1/J$ (i, j, $l = 1,\ldots, J-1$). For any triplet $\{a_i, b_j, k_l\}$, the governing equations are integrated numerically (by the Runge–Kutta method with the step $|\Delta\epsilon| = 1.0 \times 10^{-5}$).

Eqs. (25), (27) and (29) are integrated from $\sigma = 0$ to $\epsilon = \epsilon_{max}$ with the coefficients a and b equal to a_i and b_j, respectively. Afterwards, Eqs. (25), (27) and (28) are integrated from $\epsilon = \epsilon_{max}$ to $\sigma = 0$ with the coefficients a and b equal to $a_+ = k_l a_+^0$ and $b_+ = k_l b_+^0$, where a_+^0 and b_+^0 are given by Fig. 6. The best-fit parameters $\overline{a}_-$, $\overline{b}_-$ and $\overline{k}_+$ are determined from the condition of minimum of $\mathcal{F}$ on the set $\{a_i, b_j, k_l\}$. Then the initial intervals [0, a_0], [0, b_0] and [0, 1] are replaced with the new intervals $[\overline{a}_+ - \Delta a, \overline{a}_+ + \Delta a]$, $[\overline{b}_+ - \Delta b, \overline{b}_+ + \Delta b]$, $[\overline{k}_+ - \Delta k, \overline{k}_+ + \Delta k]$, and the calculations are repeated. This procedure is repeated three times with $J = 10$.

After determination of a_-^0 and b_-^0 by fitting the second cycle of each stress–strain diagram, these quantities are plotted versus strain rate $|\dot{\epsilon}|$ in Fig. 7 together with their approximations by Eqs. (18). The coefficients A_{0-}, A_{1-}, B_{0-}

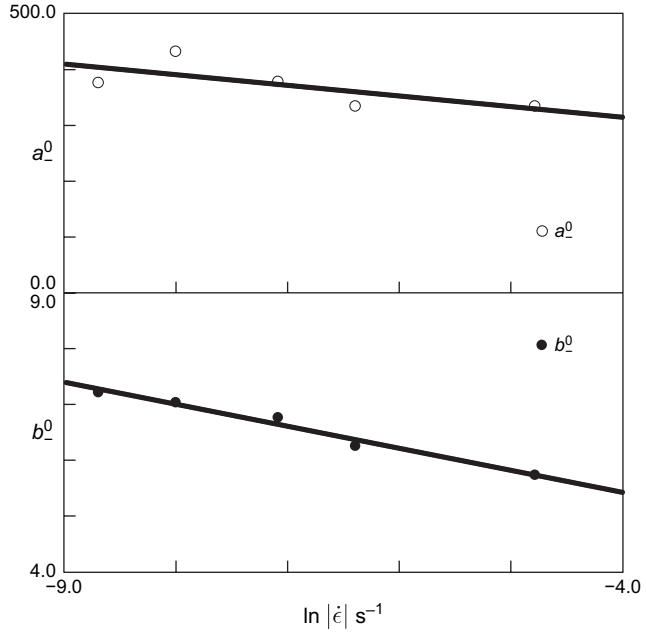

Fig. 7. Adjustable parameters a_-^0 and b_-^0 versus strain rate $\dot{\epsilon}$. Symbols: treatment of observations in cyclic tensile tests with various strain rates. Solid lines: approximation of the experimental data by Eq. (18).

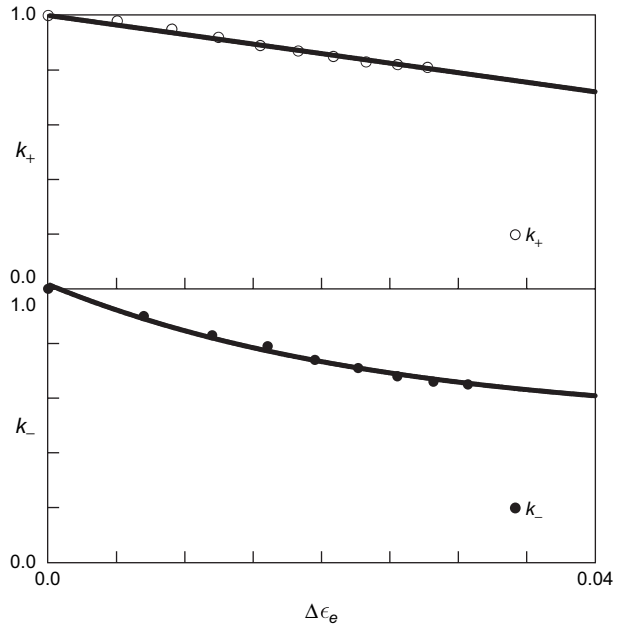

Fig. 8. Adjustable parameters k_+ and k_- versus increment of elastic strain $\Delta\epsilon_e$. Symbols: treatment of observations in a cyclic test with a strain rate of 1.7×10^{-3} s^{-1}. Solid lines: approximation of the experimental data by Eqs. (12).

and B_{1-} are found by the least-squares method and are collected in Table 1.

4.5. Other cycles of deformation

The other parts of each stress–strain curve are approximated by using a version of the above algorithm with two adjustable parameters, k_- and k_+. To fit the third cycle of deformation, for example, we fix the same intervals [0, 1] for k_- and k_+, and divide them by points $k_i = i\Delta k$ and $k_j = j\Delta k$ ($i, j = 1,\ldots, J-1$) with $\Delta k = 1/J$. For each pair $\{k_i, k_j\}$, we integrate Eqs. (25), (27) and (29) from $\sigma = 0$ to $\epsilon = \epsilon_{\max}$, and, afterwards, Eqs. (25), (27) and (28) from $\epsilon = \epsilon_{\max}$ to $\sigma = 0$. Numerical analysis is performed by the Runge–Kutta method with the step $|\Delta\epsilon| = 1.0 \times 10^{-5}$. The coefficients a and b read $a_- = k_i a_-^0$, $b_- = k_i b_-^0$ for Eq. (29), and $a_+ = k_j a_+^0$, $b_+ = k_j b_+^0$ for Eq. (28). The best-fit parameters $\overline{k}_-$ and $\overline{k}_+$ are determined from the condition of minimum of $\mathcal{F}$ on the set of pairs $\{k_i, k_j\}$. When these quantities are found, the initial intervals are replaced with $[\overline{k}_- - \Delta k, \overline{k}_- + \Delta k]$ and $[\overline{k}_+ - \Delta k, \overline{k}_+ + \Delta k]$, and the calculations are repeated. This procedure is repeated three times with $J = 10$.

The coefficients k_+ and k_- are plotted versus the increment of elastic strain $\Delta\epsilon_e$ [the difference between the current value of ϵ_e and its value ϵ_e^0 for the first retraction (reloading)] in Fig. 8. Only the data corresponding to the strain rate $1.7 \times 10^{-3}\ s^{-1}$ are reported. These data are approximated by Eqs. (12), where γ is found by the steepest descent method (in our treatment of measurements in other tests, this quantity is used without changes). The coefficients K_+ and k_-^∞ in Eqs. (12) are determined by the least-squares technique. These coefficients are independent of strain rate, and their values are collected in Table 1.

4.6. Tests with various maximum strains

We now approximate the observations in cyclic tests with a strain rate of $1.7 \times 10^{-3}\ s^{-1}$ and various maximum strains $\epsilon_{\max}$. The algorithm of fitting is similar to that applied in matching observations in tests with various strain rates. The differences between these procedures consist of the following: (i) we avoid determination of E, α and β, because these quantities have been found previously, (ii) the dependencies of a_+^0, b_+^0, a_-^0 and b_-^0 on increment of elastic strain $\Delta\epsilon_e$ are approximated by Eqs. (20), where the coefficients A_{m+}, B_{m+}, A_{m-} and B_{m-} are determined by the least-squares method, (iii) the dependencies of K_+ and k_-^∞ on increment of elastic strain $\Delta\epsilon_e$ are approximated by Eqs. (21). The entire set of material constants is reported in Table 2.

Figs. 1–3 demonstrate that the stress–strain relations correctly describe the mechanical response at all strain rates and maximum strains under consideration. According to Figs. 4–8, Eqs. (14), (15), (16), (18) and (20) adequately characterize the effects of strain rate and maximum strain on material constants.

Table 2
Adjustable parameters of the model for cyclic tests with a strain rate of $1.7 \times 10^{-3}\ s^{-1}$ and various maximum strains $\epsilon_{\max}$

Parameter	Value
E (GPa)	1.62
α	12.60
β	0.79
A_{0+}	5.66
A_{1+}	4.89
B_{0+}	4.33
B_{1+}	69.30
A_{0-}	8.24
A_{1-}	45.21
B_{0-}	4.17
B_{1-}	46.47
γ	40.70
K_{0+}	4.10
K_{1+}	34.32
K_-^∞	9.47

4.7. Accuracy of determining the material constants

A characteristic feature of cyclic deformations (which makes their analysis relatively hard) is that "averaging" of the stress–strain diagrams (measured on different samples) cannot be performed, which implies that determination of material constants should be carried out for each set of experimental data independently. This distinguishes treatment of observations in cyclic tests from that in conventional monotonic tensile tests, where several stress–strain curves obtained on different specimens can be replaced with one "average" diagram. The averaging procedure becomes questionable due to the fact that relatively small variations in apparent residual strains at retraction to the zero stress (inevitable in experiments) cause large deviations between the stress–strain curves at reloading.

To assess the level of uncertainty in calculation of material constants induced by our choice of a particular sample, we apply the above procedure of matching observations to the experimental data obtained on three independent specimens in cyclic tests with a strain rate of $1.7 \times 10^{-3}\ s^{-1}$ and a maximum strain of 0.1. The average values of material constants and their maximum (not standard) deviations are listed in Table 3 (to simplify the numerical analysis, the same values of E, α and β are used). Table 3 shows that the accuracy of finding the adjustable parameters is relatively high: the maximum deviations do not exceed 11%. This level of accuracy coincides

Table 3
Average values of material parameters and their maximum deviations for a cyclic test with a strain rate of $1.7 \times 10^{-3}\ s^{-1}$ and a maximum strain of 0.10

Parameter	Average value	Maximum deviation (%)
a_+^0	226.00	11
b_+^0	3.04	5
a_-^0	656.00	6
b_-^0	1.06	4
K_+	12.02	4
k_-^∞	0.39	6

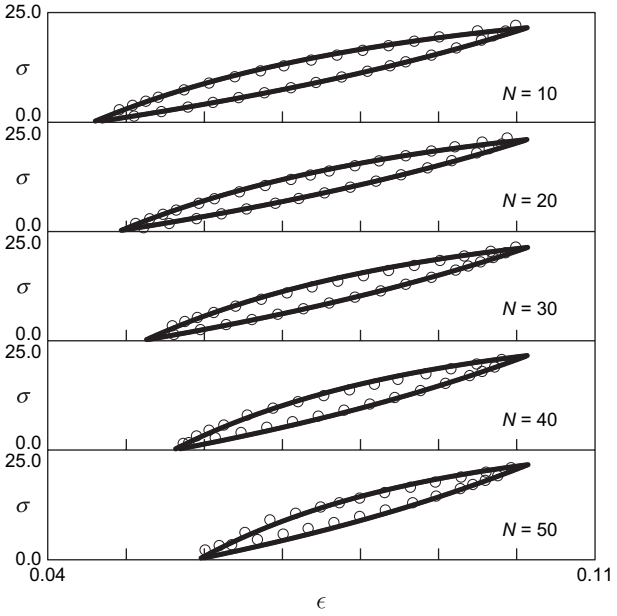

Fig. 9. The engineering stress σ versus engineering strain ϵ at the Nth cycle ($N = 10$, 20, 30, 40, 50). Circles: treatment of observations in a cyclic test with a strain rate of 1.7×10^{-3} s^{-1} and a maximum strain of $\epsilon_{max} = 0.10$. Solid lines: results of numerical simulation.

with that conventionally accepted for the Young's modulus of solid polymers evaluated by standard methods.

4.8. High-cycle deformation programs

Unlike the above analysis focusing on deformation programs with $N = 10$ cycles, our aim now is to examine the model predictions when the number of cycles N becomes relatively large. For this purpose, an additional cyclic tensile test was performed with the strain rate 1.7×10^{-3} s^{-1}, the maximum strain $\epsilon_{max} = 0.1$, and the number of cycles $N = 50$. The material parameters are found following the above procedure of matching observations. The experimental stress–strain diagrams for the 10, 20, 30, 40 and 50th cycles are depicted in Fig. 9 together with the results of numerical simulation (approximation at $N = 10$, 20, 30, 40 and prediction for $N = 50$). This figure shows that the constitutive model correctly fits the observations and adequately predicts the mechanical response. According to Fig. 9, the apparent residual strain at retraction increases, whereas the maximum stress per cycle decreases with number of cycles. The growth of the apparent residual strain occurs more pronouncedly (43%) than the reduction in the maximum stress (9%).

The only difference between the low-cycle and high-cycle deformation programs is observed in Fig. 10, which demonstrates that k_+ and k_- reach their ultimate values k_+^∞ and k_-^∞ when the increment of elastic strain $\Delta\epsilon_e$ exceeds its critical value $\Delta\epsilon_e^{cr} \approx 0.04$.

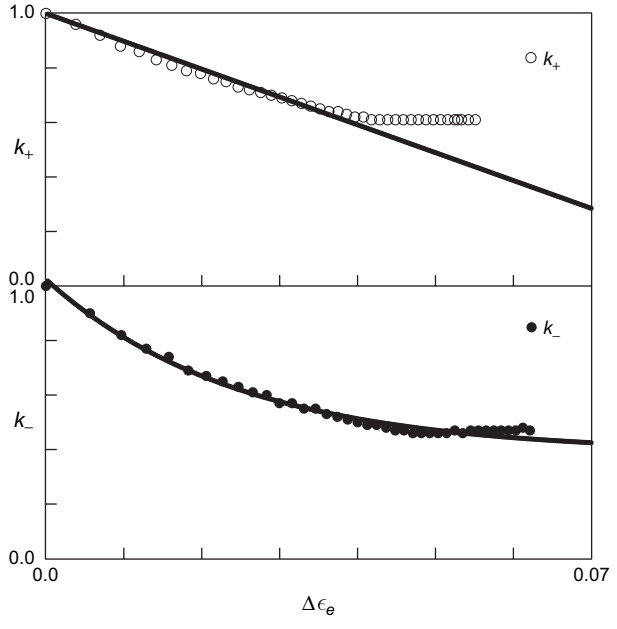

Fig. 10. Adjustable parameters k_+ and k_- versus increment of elastic strain $\Delta\epsilon_e$. Symbols: treatment of observations in a cyclic test with the maximum strain $\epsilon_{max} = 0.10$. Solid lines: approximation of the experimental data by Eqs. (12).

5. Concluding remarks

Experimental stress–strain diagrams are reported on polypropylene random copolymer at uniaxial cyclic tensile deformations with various strain rates and maximum strains (that cover the entire interval of strains below the necking point). By using the laws of thermodynamics, constitutive equations are derived for the viscoplastic response of a solid polymer at arbitrary three-dimensional deformations with small strains. Adjustable parameters in the stress–strain relations are found by fitting the experimental data. It is shown that (i) the model correctly describes the observations and (ii) the material parameters change consistently with amplitude and rate of cyclic deformations.

References

[1] Bai SL, Wang M. Polymer 2003;44:6537–47.
[2] Shen XH, Xia ZH, Ellyin F. Polym Eng Sci 2004;44:2240–6.
[3] Christenson EM, Anderson JM, Hiltner A, Baer E. Polymer 2005;46:11744–54.
[4] Prisacariu C, Buckley CP, Caraculacu AA. Polymer 2005;46:3884–94.
[5] Pruitt LA. Biomaterials 2005;26:905–15.
[6] Yi J, Boyce MC, Lee GF, Balizer E. Polymer 2006;47:319–29.
[7] Bergstrom JS, Boyce MC. Mech Mater 2001;33:523–30.
[8] van Dommelen JAW, Parks DM, Boyce MC, Brekelmans WAM, Baaijens FPT. J Mech Phys Solids 2003;51:519–41.
[9] Bergstrom JS, Rimnac CM, Kurtz SM. Biomaterials 2004;25:2171–8.
[10] Bergstrom JS, Hilbert LB. Mech Mater 2005;37:899–913.
[11] Drozdov AD, Christiansen JdeC. Mech Res Commun 2003;30:431–42.
[12] Drozdov AD, Christiansen JdeC. Polym Eng Sci 2004;44:548–56.
[13] Kletschkowski T, Schomburg U, Bertram A. Mech Mater 2002;34:795–808.
[14] Kletschkowski T, Schomburg U, Bertram A. Mech Mater 2005;37:687–704.
[15] Ho K, Krempl E. Int J Plasticity 2002;18:851–72.
[16] Colak OU. Int J Plasticity 2005;21:145–60.
[17] Lai D, Yakimets I, Guigon M. Mater Sci Engng A 2005;405:266–71.

[18] Mizuno M, Sanomura Y. J Soc Mater Sci Japan 2005;54:414–9.
[19] Oshmyan V, Patlazhan S, Remond Y. J Mater Sci 2004;39:3577–86.
[20] Remond Y. Compos Sci Technol 2005;65:421–8.
[21] Fujisawa N, Swain MV. J Mater Res 2006;21:708–14.
[22] Ogden RW, Roxburgh DG. Proc R Soc London A 1999;455:2861–77.
[23] Kolarik J, Pegoretti A. Polymer 2006;47:346–56.
[24] El-Farahaty KA. Polym Test 1996;15:163–77.
[25] Drozdov AD, Christiansen JdeC. Int J Solids Struct 2007;44:2677–94.
[26] Richeton J, Schlatter G, Vecchio KS, Remond Y, Ahzi S. Polymer 2005;46:8194–201.
[27] Subhash G, Liu Q, Gao X-L. Int J Impact Engng 2006;32:1113–26.
[28] Richeton J, Ahzi S, Vecchio KS, Jiang FC, Adharapurapu RR. Int J Solids Struct 2006;43:2318–35.
[29] Dorfmann A, Ogden RW. Int J Solids Struct 2003;40:2699–714.